11

Basic Mechanisms for Single Atom Manipulation in Semiconductor Systems with the FM-AFM

Pablo Pou, Pavel Jelínek, and Rubén Pérez

Abstract. This chapter unveils the atomic-scale mechanisms that are responsible for the room temperature manipulations of strongly bound atoms on semiconductor surfaces. First-principles simulations, matching the experimental forces, identify the key steps in two paradigmatic examples: the lateral manipulation of single adatom vacancies on the Si(111)-7×7 reconstruction in the attractive regime and the vertical interchange of atoms between the tip and the Sn/Si(111)-($\sqrt{3}\times\sqrt{3}$)R30° surface by a gentle exploration of the repulsive force regime. Our calculations reveal that the outstanding experimental control of the manipulation under attractive forces comes from the localized reduction of the diffusion energy barriers induced by the tip for the different steps in the complex path followed by the Si adatom during the process. Using selective constraints, to face the difficulties posed by the complexity of a multi-atom contact and operation in the repulsive regime, our simulations illustrate how the vertical interchange can take place at the atomic scale, identify the crucial dimer structure formed by the closest tip and surface atoms, and discuss the role of temperature in the competition with other possible final outcomes (including atom removal or deposition by the tip).

11.1 Introduction

Scanning probe microscopes (SPM) have become the tool of choice for imaging and manipulation at the nanoscale. During SPM operation, the forces appearing due to accidental contact may lead to changes in the tip and surface structure. This experimental observation has triggered the efforts to convert the tip-induced removal, deposition, and lateral displacement of atoms into a controlled manipulation process, where the final outcome of the process can be determined at will with atomic-scale precision. Just a decade after the development of the scanning tunneling microscope (STM), Eigler and Schweizer started the era of man-made atomic patterns manipulating Xe atoms on an Ni(111) surface at cryogenic temperatures to form the IBM logo [1]. While

S. Morita et al. (eds.), *Noncontact Atomic Force Microscopy*,
NanoScience and Technology,
DOI: 10.1007/978-3-642-01495-6_11,

atomic-scale manipulations with the STM under low-temperature (LT) conditions have become routine in many laboratories, progress with the atomic force microscope (AFM) was hampered by the limitations in resolution.

The first atomically resolved images of the Si(111)-7×7 reconstruction taken with the AFM operated in the frequency modulation mode (FM-AFM, also known as noncontact AFM) [2] were published in 1995. After this breakthrough, it took only 7 years for the FM-AFM, operating at 78 K, to show its ability to remove single adatoms from this reconstruction and to fill these vacancies again with Si atoms coming from the tip [3] (see Fig. 11.7). At variance with similar experiments with the STM, no bias voltage or voltage pulse was involved in these atomic manipulations as both tip and sample were always electrically grounded. They are purely mechanical, and rely only on the exquisite control of the tip–sample interaction to extract from the surface a single adatom that is strongly connected by three covalent bonds to the underneath Si layer. These manipulations were followed by experiments at room temperature from two groups [4, 5] on the same surface. In 2005, lateral atomic manipulations at both LT and room temperature (RT) were reported on Ge(111) surfaces [6]. These experiments proved that adsorbates, as well as intrinsic adatoms of semiconductor surfaces, could be individually manipulated laterally using the tip–sample short-range interaction force. The interchange lateral manipulation of substitutional Sn adatoms – that are not mobile on the Ge surface at RT – allowed the formation of artificial nanostructures that are stable at RT [7]. Basic atomic manipulations at RT have also been achieved on insulating surfaces [8, 9].

The very precise control of the position of the tip-apex even at RT [10–12] as well as the ability to measure the tip–sample interaction in force spectroscopy experiments with outstanding accuracy (see [13, 14] and Chap. 3) are behind the recent breakthroughs in FM-AFM manipulation: (1) The atomistic mechanism involved in the lateral manipulations at RT – the local tuning of energy barriers for tightly-bound atoms to allow thermally induced displacements – has been identified and put on a firm, quantitative basis by a combined theoretical and experimental study on the Si(111)-7×7 surface [15]; (2) The force required to move an atomic adsorbate on a metallic surface at LT has been determined [14]; and (3) an atomic dip-pen lithography technique based on the vertical interchange of single atoms between the tip-apex and the topmost layer of a semiconductor surface at RT has been developed [16].

All of the atomic manipulations mentioned so far can be grouped in terms of the character of the tip–sample interaction: lateral manipulations are performed in the attractive regime, while the deposition or removal of surface atoms and the vertical interchange correspond to the repulsive regime of the short-range interaction. The goal of this chapter is to unveil the atomic-scale mechanisms that are responsible for the RT manipulations of strongly bound atoms on semiconductor surfaces and to characterize the basic properties of the two interaction regimes. Our approach is based on a set of carefully designed, large-scale first-principle simulations. At variance with STM,

FM-AFM provides direct access to the forces during the manipulation process. This information can be exploited to reproduce the experimental conditions in our simulations, matching quantitatively the theoretical forces and those measured in force spectroscopy experiments.

The rest of the chapter is organized as follows: In Sect. 11.2, we summarize our theoretical approach for the calculation of the optimal atomic pathway in different manipulation processes. A detailed analysis of the interaction between a semiconductor surface and a silicon tip is provided in Sect. 11.3. Section 11.4 describes the study of the lateral manipulation of single adatom vacancies on the Si(111)-(7×7) surface at room temperature performed in the attractive interaction regime. In Sect. 11.5, we report theoretical simulations of the vertical atomic exchange taking place between the tip and sample in the strong-repulsive interaction regime.

11.2 Theoretical Approach: First-Principles Simulations

Atomic manipulations are directly accompanied by the breaking and formation of chemical bonds between the different atoms involved in the process. The inherent quantum character of the chemical bonding requires the use of first-principles methods based on density functional theory (DFT). Furthermore, atomic manipulations, mainly those performed in the repulsive regime, involve many atoms of both the surface and the probe. This multi-atom contact significantly increases the number of possible trajectories and their complexity in the configuration space. The efficient characterization of the potential energy surface (PES) and the search for optimal trajectories are challenging tasks that have attracted a lot of attention during the last few years [17, 18].

Although several theoretical studies on atomic manipulation with FM-AFM [19, 20] have been carried out with a fully converged first-principles description using plane-wave (PW) DFT methods, an extensive search of the PES using PW methods is still precluded by their large computational demand. An interesting alternative is to resort to DFT methods based on a local orbital basis, specially those developed with the aim of computational efficiency, that allow first-principles studies of much more complex systems and trajectories. In the simulations presented in this chapter, we have used a fast local-orbital DFT-LDA technique (Fireball) [21,22]). This approach offers a very favorable accuracy/efficiency balance once the atomic-like basis set is carefully chosen [23].

We model the real tip–surface system using a supercell approach. In the simulations described later, the Si(111)-(7×7) and the Sn/Si(111)-$(\sqrt{3} \times \sqrt{3})$ reconstructions were represented by a (7×7) and a (6×6) periodic slab that includes 7 Si layers and a total of 347 and 264 atoms, respectively. Due to the

large size of these surface unit cells, only the Γ point was used to sample the Brillouin zone.

The modeling of the tip is one of the key issues in AFM. This is a complex problem, where the lack of direct experimental information on the structure after tip preparation combines with the possibility of surface contamination during the AFM operation. Our long experience with semiconductor surfaces shows that, to simulate processes where the tip-apex does not interact strongly with the surface, i.e., in the attractive regime, a tip model that fairly reproduces the chemical reactivity of the few outermost atoms of the apex is appropriate. In particular, we have shown [13, 15, 24, 25] that it is possible to characterize the most probable structure and composition of the apex by a detailed comparison between the attractive short-range (SR) forces obtained in first-principles simulations with the experimental ones. However, in the strong-interaction regime, the role of the mechanical response of the tip becomes more important, and larger models would be required for a complete, quantitative study. This problem is further discussed in the context of the vertical manipulations presented in Sect. 11.5.

The vertical scanning operation in AFM was simulated in a stepwise, quasi-static manner by making small movements of the tip perpendicularly to the surface. The atoms of both tip and surface were allowed to relax to their ground state configuration – with convergence criteria for the total energy and forces of 10^{-6} eV and $0.05\,\mathrm{eV\AA^{-1}}$, respectively – at each of these steps. Only the slab last layer with H atoms saturating it and the topmost part of the tip model were kept fixed. The quasi-static approximation provides a very good description of the imaging process due to the fact that the motion of AFM tip is much slower than the ongoing atomic processes in the system.

11.3 The Short Range Chemical Interaction Between Tip and Sample

Imaging [13,26] and manipulation [5,14,15,19] mechanisms on semiconductor and metal surfaces are mostly determined by the short-range chemical interaction between a surface atom and the outermost atoms of the probe. Therefore, a detailed knowledge of the character of the chemical forces acting between the tip and the sample, and its dependence on the tip–sample distance and their atomic and electronic structure, is a key ingredient to understand and control these processes.

Semiconductor surfaces often undergo a strong structural rearrangement of the upper surface atomic layers, with respect to an ideal surface, to minimize the number of unsaturated bonds – the so-called *dangling bonds* – and lower the total energy. Taking the Si(111)-7×7 case as an example, the reconstruction leaves only 12 adatoms in the upper layer, reducing the original 49 dangling bonds to only 19 (located on the 12 adatoms, the six rest atoms

in the second layer and the corner hole). These *dangling bond* states determine the strong chemical activity of most semiconductor surfaces. The atomic resolution obtained on semiconductors with the FM-AFM [26] was precisely attributed to the presence of a *dangling bond* state on the outermost atom of the silicon tip that interacts with the dangling bonds on the surface.

The strong covalent bonding of surface atoms in semiconductors significantly reduces their mobility and, therefore, to manipulate them, larger mechanical forces, used for weakly bound adsorbates on metal surfaces, are required. However, this problem in the manipulation process turns into an asset when considering stability issues: the strong interaction significantly extends the lifetime of the formed atomic patterns, and allows the existence of these assemblies at RT, which makes them much more relevant for technological applications. To illustrate the strength of the chemical interaction between the *dangling bonds* of a prototypical semiconductor tip and a surface adatom, we present results of a DFT simulation for the system considered in our study of the lateral manipulation (see Sect. 11.4): a corner Si adatom on the Si(111)-(7×7) reconstruction with a vacancy in the adjacent central adatom position in the half-unit cell. Due to the localized character of the interaction, these results can be generalized to an arbitrary semiconductor surface with strongly localized *dangling bonds*.

Figure 11.1 shows the evolution with the tip–sample distance of the atomic and electronic structure. At large tip–sample distances, there is a negligible vertical displacement of the adatom (see the left top plot in Fig. 11.1). A sudden upward movement of the adatom of $\sim$0.4 Å is observed for a tip–sample distances of $\sim$4.5 Å. A strong correlation between the onset of the short-range chemical force between tip and sample and the vertical displacement of the adatom can be clearly identified in the middle graphs in Fig. 11.1. Next, the vertical adatom displacement decreases until it reaches its initial value at a tip–sample distance near to 2.5 Å while, at the same time, the SR force increases linearly. A further decrease of the tip–sample distance, below 2 Å, induces substantial atomic rearrangements as too much elastic energy has been already stored in few bonds (for details see Fig. 11.6 and the discussion in Sect. 11.5).

These changes in the structure are coupled with significant changes in the electronic properties. A detailed analysis of the density of states projected on the adatom along the tip–sample distance (see Fig. 11.1) points out a strong modification of the *dangling bond* state [27]. In the far-distance regime, the dangling bond state remains in a similar energy as on the unperturbed surface. Reaching tip–sample distances of $\sim$4.5 Å, where the onset of the chemical bond between tip and sample takes place, we observe a strong modification of the local electronic state of the inspected surface adatom. At closer tip–sample distances, below 4.5 Å, the dangling bond state is completely wiped off from the Fermi level, as it can be seen in Fig. 11.1. These electronic modifications have significant implications for the transport properties as discussed in [27].

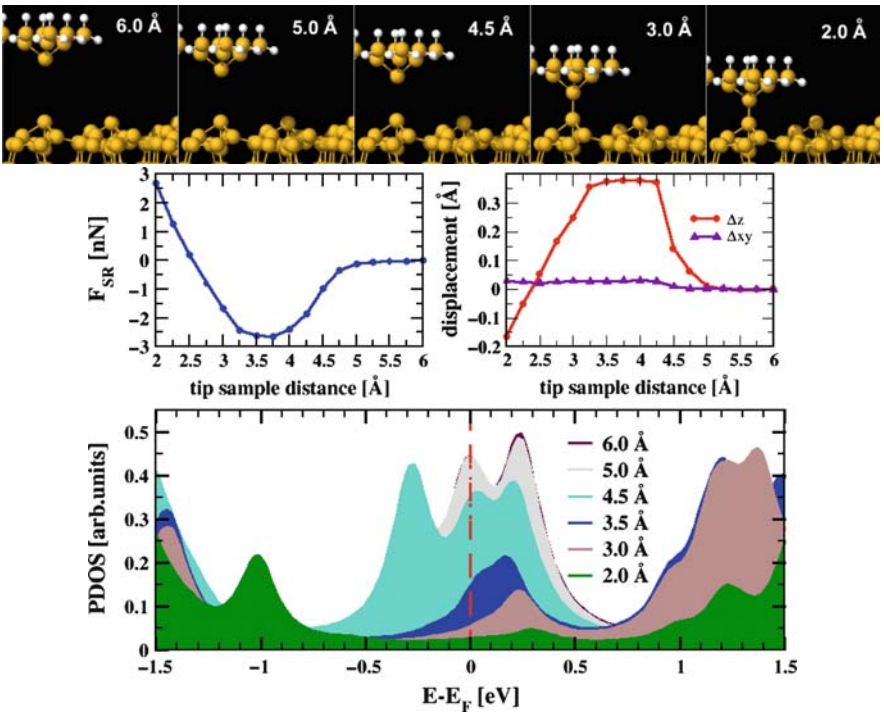

Fig. 11.1. (*Top*) Relaxed atomic structures at different tip–sample distances during the approach of a silicon tip toward a corner adatom on the Si(111)-(7 × 7) surface. (*middle*) Short-range force (*left*) and vertical and lateral displacement of the adatom (*right*) as a function of the tip–sample distance. (*bottom*) Projected density of states (PDOS) on the Si adatom below the tip apex at different tip–sample distances

To summarize, we have seen how the proximity of the tip and the consequent formation of the chemical bond between the outermost apex atom and the surface adatom, induces a strong modification of the atomic and electronic structure of the intrinsic adatom states on semiconductor surfaces. This effect leads to a weakening of the adatom surface bonds and, therefore, it facilitates its eventual transfer on the surface, as in further sections.

11.4 Manipulation in the Attractive Regime: Vacancies in the Si(111)-(7 × 7) Reconstruction

The vacancy-mediated lateral manipulation of intrinsic Si adatoms on the Si(111)-(7 × 7) surface at room temperature [15], represents a paradigmatic example of atomic manipulation performed in the attractive tip–sample interaction regime. A precise command of both the vertical and lateral position of the probe allows the controlled movement of individual Si adatoms on

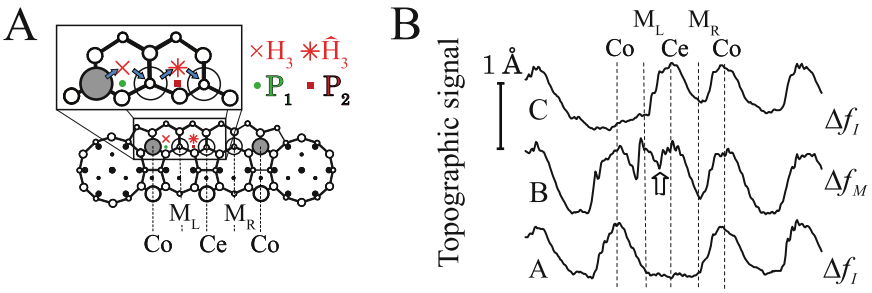

Fig. 11.2. (**a**) The optimal atomic pathway during the Co→Ce manipulation. (**b**) Topographic signals taken at different stages of the manipulation process obtained in two different, low (Δf_I) and high interaction (Δf_M), set points

semiconductor surfaces (see Fig. 11.2). The manipulation was performed using an experimental protocol similar to the one reported in [7] and described in Chap. 8: the process of imaging and manipulation itself was controlled by switching between a weaker (Δf_I) and a stronger interaction (Δf_M) set point while scanning along the direction of the desired movement (see Fig. 11.2b). Constant-frequency shift profiles A–C in Fig. 11.2b correspond to consecutive scans moving the tip from left to right over the same line of the surface. Profile A has been obtained before the manipulation at the low-interacting set point, Δf_I. The vacancy placed in the central (Ce) adatom position can be clearly identified. Profile C shows the position of the atoms after the manipulation: the corner (Co) adatom has been displaced to the center adatom position. Profile B, acquired at the stronger tip–sample interaction regime (Δf_M), corresponds to the manipulation process. This profile clearly illustrates that the single-atom manipulation process involves, at least, two consecutive jumps between adjacent sites: CoA → M and M → CeA (see Fig. 11.2a). The maximal attractive short-range force needed to move the silicon adatom, experimentally determined for the Δf_M operating conditions, was ∼0.5 nN. Notice that, in principle, a larger value – closer to the maximum strength of the covalent bonds between the adatom and the surface – could be expected.

To obtain a detailed picture of the atomic-scale processes involved in the lateral manipulation, we have carried out an analysis of the optimal atomic pathways using first principles DFT methods. We have considered the case illustrated in Fig. 11.2: an Si(111)-7 × 7 reconstruction, where an adatom initially located on the Co site is transferred to the Ce empty site. The PES for the vacancy pathway was characterized through an extensive set of DFT simulations, including the determination of the energetics for the vacancy on different adatom sites and the activation energy barriers for the adatom hopping toward available empty sites. To estimate the magnitude of the activation energy barriers on the surface, we have used a quasi-static approach where the adatom is moved in discrete steps along the most energetically favorable trajectory between two adjacent local minima, letting the system to relax to its

ground state keeping the adatom lateral (x, y) coordinates fixed. These calculations reveal that the apparent two-step manipulation is actually a much more complex process. We have identified the path $Co \rightarrow H_3 \rightarrow M_L \rightarrow \hat{H}_3 \rightarrow Ce$ (see Fig. 11.2a) as the optimal pathway to move the adatom from the Co site to the empty Ce site. The magnitude of the activation energy barriers of the individual jumps along the optimal trajectory, estimated from our constrained minimization calculations, are summarized in Fig. 11.3a. The large energy barriers for some of the steps (e.g., $> 1.5\,\text{eV}$ for the $Co \rightarrow H_3$ step) practically forbid the thermally activated diffusion of adatoms at RT, in agreement with the experimental observations under the normal imaging conditions (using the Δf_I set point).

In Sect. 11.3 we have shown how the proximity of a silicon tip weakens the adatom bonds with its neighboring surface atoms. It is evident that this effect must play a crucial role in the lateral manipulation processes discussed here. Therefore, we have analyzed in detail the influence of the tip–sample interaction (as determined by the relative position of the tip and the adatom) on the barriers associated with the different jumps in the adatom pathway from the Co to the Ce site. For these simulations, a well-tested Si(111) nanoasperity [26] was used as tip model. This tip, although small and consequently fairly rigid, correctly reproduces the *dangling bond* termination of the Si tips used in the experiments. In particular, this tip matches quantitatively the measured forces and provides a fairly symmetric interaction, in agreement with the experimental observation that identical Δf_{M} operating conditions are needed for manipulating the adatom in different directions. As shown later, these are the key ingredients to reproduce the role played by the tip in the atomic manipulations performed in the attractive regime. Nevertheless, other tip-apex structures (as the tip model showed in Fig. 11.9) were also tested. No significant differences with the results for the tip considered here were found.

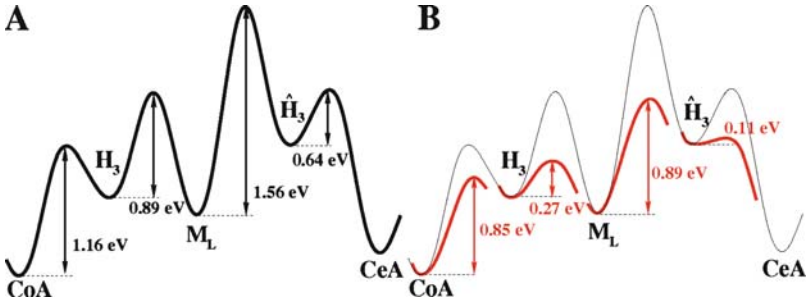

Fig. 11.3. (**a**) Energy barriers along the optimal atomic pathway for the diffusion of a silicon atom from the Co to the Ce site on the Si(111)-(7×7) without the presence of a tip. (**b**) Change of the energy barriers along the optimal atomic pathway induced by the proximity of a silicon tip at the tip–sample distance of 4.0 Å.

To estimate the influence of the tip on the energy barriers, we have performed a large set of constrained minimizations for several tip–sample distances and different tip lateral positions. Notice that during the energy minimization procedure all the atoms in the tip, apart from the last Si layer and the saturating H-layer, are allowed to relax. Figure 11.4 illustrates the reduction of the activation energy barriers with the increasing tip–sample interaction in the case of the two most difficult steps, the $Co \rightarrow H_3$ and the $M_L \rightarrow \hat{H}_3$, with the tip placed in the P_1 and P_2 horizontal positions respectively (see Fig. 11.2a). These points are located on the scan line followed during the manipulation experiments. Similar tendencies can be found in both cases: the reduction of the tip–sample distance below 4.5 Å is accompanied by a substantial reduction of the activation energy barriers. A total energy lowering of the final metastable positions, H_3 and $\hat{H}_3$ respectively, is also observed.

We have quantified the role of the horizontal position of the tip in the mechanism of the lateral adatom manipulation. We have calculated the activation energy barriers of the $Co \rightarrow H_3$ step varying the lateral position of the tip, see Fig. 11.5, while the tip height was kept constant at $z = 4.0$ Å. Figure 11.5a displays the change of the barrier according to the variation of the tip position in the direction perpendicular to the scan movement. Along this direction, only minor variations of the activation barrier are observed. However, the variation of the horizontal tip position in the direction from the Co to the H_3 site (see Fig. 11.5b), shows more dramatic changes in both the magnitude of the barrier and the total energy of the final state.

The results presented earlier provide a clear indication of the basic mechanism operating during atomic manipulations in the attractive regime. As Figs. 11.4 and 11.5 show, for tip–surface distances corresponding to calculated SR forces around the experimental values used during the manipulations, the barriers are reduced close to the value (∼0.8 eV) that enables spontaneous

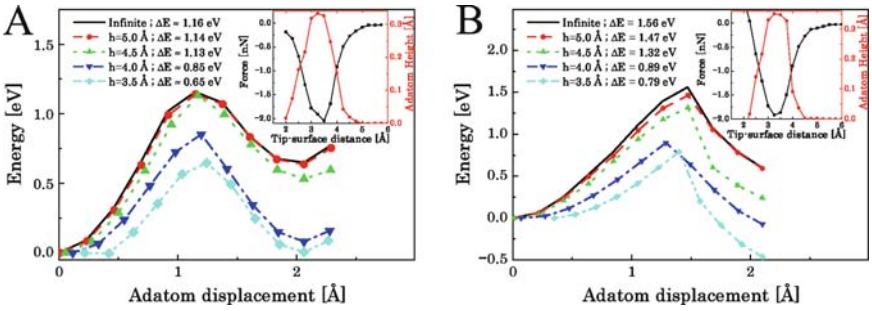

Fig. 11.4. Calculated diffusion barriers for the (**a**) $CoA \Rightarrow H_3$ and (**b**) $M \Rightarrow \hat{H}_3$ steps, when the tip is located at the P_1 and P_2 positions (see Fig. 11.2) at different tip–sample distances. The insets show the short-range force and the vertical displacement of the silicon surface adatom as a function of the tip–sample distance

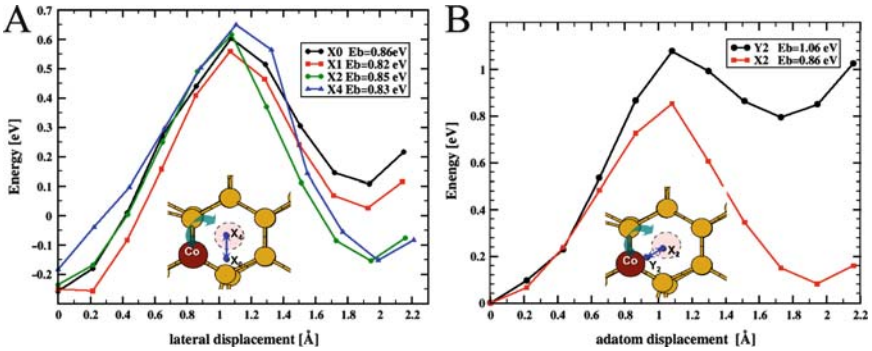

Fig. 11.5. Calculated diffusion barriers for the $CoA \Rightarrow H_3$ step for different horizontal tip positions (shown in the inset). The tip height was fixed, in all cases, at 4.0 Åwith respect to the corner Si adatom of the Si(111)-(7×7) faulted unit cell

thermally activated jumps between the two sites at RT during the long time (for typical oscillation frequencies around 100 kHz) that the tip spends close to the sample. Similar significant reductions on the calculated energy barriers (see Fig. 11.3) are also found for the rest of the transitions between adjacent adsorption sites when the tip is located close to the relevant lateral position along the manipulation path where the adatom jumps are observed.

This mechanism based on thermally activated hopping, already proposed for previous STM manipulation experiments, is now put on a firm quantitative basis. Surprisingly, our simulations confirm the experimental observation that atomic manipulations are possible at tip–samples forces that are quite small compared to the strength of the semiconductor covalent bonds. The explanation lies on the thermal energy available at RT and the long tip residence times. This combination allows a precise control of the atomic jumps by means of tip assisted diffusion, fine tuning the interaction strength through the tip–sample distance for a range of operating temperatures. Notice that this precise command on the atomic jumps would not be possible without the strong localization of the energy barrier reduction induced by the "sharp" *dangling bond* of the outermost atom of the tip, as illustrated by the results showed in Fig. 11.5. Blunter tips would reduce several barriers at the same time, making the controlled manipulations much more difficult. The unique combination of sharp tips and precise experimental control of the tip position found in FM-AFM, where the apex can be placed in a specific point to induce an atomic jump over a particular energy barrier, provides access to the atomic-scale manipulation at RT.

In summary, our DFT simulations have revealed the key for controlled lateral manipulation: the substantial local reduction of the diffusion energy barriers. The onset of significant attractive forces below 5 Å, directly associated with the covalent interaction between the tip and surface dangling bonds, induces pronounced vertical relaxations on the adatom (see the insets

of Fig. 11.4), the surrounding surface atoms and the outermost tip atoms. By gently tuning this interaction, it is relatively easily to reduce these barriers below the limit that enables instantaneous thermally activated diffusion at RT. The control of the net adatom displacement is then possible using the directionality imposed by the tip global movement.

11.5 Manipulation in the Repulsive Tip–Surface Interaction Regime

11.5.1 A Complex Phase Space Under Strong Tip–Surface Interactions

The theoretical simulation of the vertical manipulation processes described in Sect. 11.1 – and, in particular, the vertical atom interchange discussed later in Sect. 11.5.2 – represents a formidable challenge. These manipulations are produced by the gentle exploration of the repulsive part of the short-range chemical interaction between the closest tip–surface atoms. At variance with the simulations for lateral manipulation described so far, it is necessary to face the problems associated with working in the repulsive regime of the tip–surface short-range interaction and the intrinsic complexity of the phase space associated with a multi-atom contact. We understand, from our previous work on force spectroscopy [13], that the slope of the repulsive part of the interaction, that is controlled by the effective combined stiffness of the tip and surface, varies significantly for different tips on different experimental sessions. Our first-principles calculations for tips with quite different apex structure and chemical composition (even for large tips including 48 Si atoms) show a much smaller variability, with effective stiffnesses consistently larger than the experimental results. This systematic behavior is due to the constraint of fixed atomic positions for the last atomic layer of the tip imposed in first-principles calculations: we are losing the long-range elastic response of the tip, that is not dominated by the apex. One could argue that with an atomistic approach with classical potentials, we can consider much larger tips models and fix this problem with the elastic response. Unfortunately, these potentials performed very poorly in the description of the breaking and remaking of bonds that necessarily lies behind the vertical manipulation. This is the reason why we choose to stick to first-principles calculations, sacrifice the precise, quantitative description of the tip–elastic response, and focus on providing some clues about the feasibility of these processes and the atomic mechanisms involved.

To start the study of the relevant configurations that the closest tip and surface atoms can explore in this strong interaction regime, we first analyze the atom removal or deposition by the tip on the Si(111)-(7×7) achieved in the first FM-AFM manipulation experiments (see Fig. 11.7e, f). To this end, we have considered the same Si tip used in our simulations of the lateral manipulation in the attractive regime. We have performed DFT simulations

approaching the tip towards the Si(111)-(7×7) surface and then retracting the tip back to the starting position. These simulations illustrate how the removal of the adatom from the surface takes place at the atomic scale.

Our results for the case, where the tip-apex atom is positioned right on top of one of the corner adatoms are shown in Fig. 11.6. In the first steps of the tip excursion toward the surface, the system explores the attractive interaction regime discussed in detail in Sect. 11.3. Reducing the tip–sample distance further, below 2 Å, the apex atom is pushed into the tip (see Fig. 11.6b), increasing the mechanical strain of the system. At even closer tip–sample distance, ∼0.5 Å, the system is no longer able to sustain the applied mechanical load: it undergoes a substantial rearrangement of atoms in the contact area between tip and sample to minimize its total energy and to release the mechanical stress. The irreversible atomic deformation manifests in the characteristic jump in the total energy vs. distance. We should emphasize that, until reaching point B, the response of the system to the mechanical load is purely elastic and during tip retraction, the system returns to the original configuration with no significant energy dissipation [24,28]. However, crossing point B, a plastic deformation – associated with the breaking of few bonds where the stress was accumulated during the loading – takes place. The system no longer matches the original pathway on retraction and it undergoes different atomic rearrangements. On further retraction, a characteristic *dimer-like* structure with the apex atom and the surface adatom (see Fig. 11.6e) is formed. Finally, the adatom is picked up by tip (Fig. 11.6f) and removed from the surface.

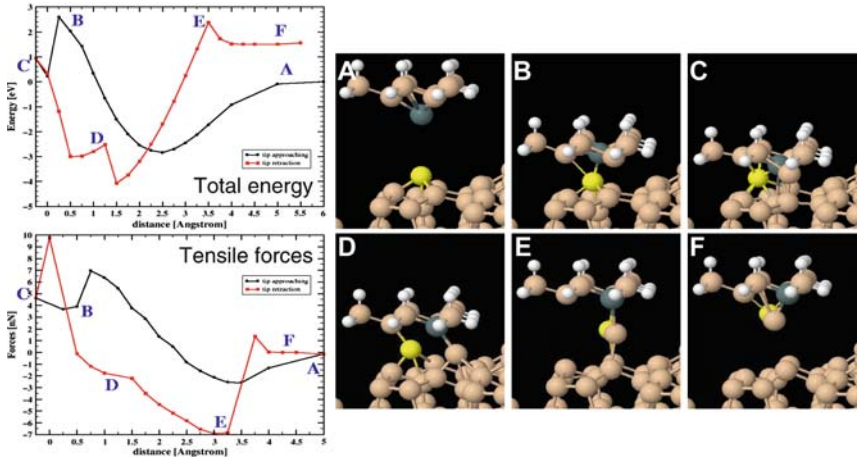

Fig. 11.6. Atomic pathway for the adatom extraction process: (*left*) Total energy and short-range force along the approach/retraction cycle of a Si tip over a corner silicon adatom on the faulted unit cell in the Si(111)-(7×7) surface. (*right*) Snapshots (**a**–**f**) show the evolution of the atomic structure during the approach (A–C) and the retraction (C–F)

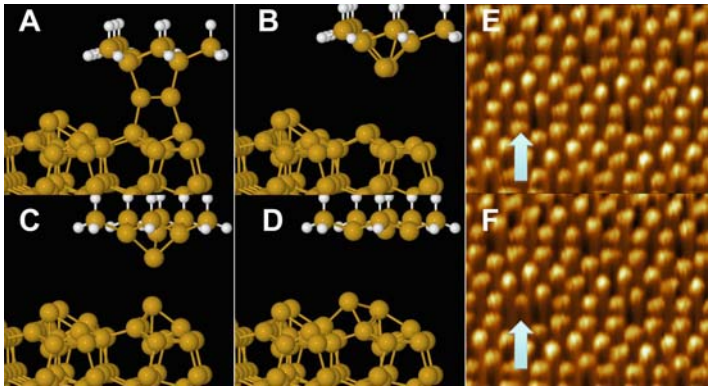

Fig. 11.7. Complexity of the phase space in the strong interaction regime. (**a**) Characteristic *dimer-like* structure that minimizes the energy of a tip–surface system at close tip–sample distances. (**b**)–(**d**) Possible final atomic structures after the tip approach/retraction cycle: (**b**) the tip extracts the surface adatom, (**c**) the tip and the surface keep their original structure, and (**d**) a tip atom is deposited on the surface. (**e**) and (**f**) the experimental formation of an atomic vacancy on the Si(111)-(7×7) surface using FM-AFM (for details, see [3]). The *arrows* mark the place where the manipulation process took place

The *dimer-like* configuration found in the process (Fig. 11.6e, and clearly illustrated in Fig. 11.7a), is very interesting, because it represents a bifurcation point in the phase space. This basic motif appears in all of the simulations that we have performed, starting from different initial conditions. However, from this atomic configuration, the system can branch out into quite distinct areas of the configuration space corresponding to different local energy minima and atomic structures. Our simulations show that, depending on several factors such as the initial tip position and the indentation depth, the system can reach, without crossing significant energy barriers, different final configurations on retraction. These possible scenarios include (1) the extraction of a surface adatom (Fig. 11.7b), (2) the return to the initial configuration (Fig. 11.7c), and (3) the deposition of a tip atom on the surface (Fig. 11.7d). These results illustrate, even with this relatively simple tip, the complexity of the phase space when exploring the repulsive regime, where subtle differences in the bonding configuration of the basic dimer structure lead to markedly different outcomes of the approach/retraction process. The presence of several atomic species further enlarges the phase space. As discussed in Sect. 11.5.2, the dimer motif plays also a central role in the microscopic understanding of the vertical atom interchange experiments performed at room temperature (Fig. 11.8), where a surface atom is replaced by a tip atom of a different chemical species after an approach/retraction cycle. This analysis will require the inclusion of temperature effects in the competition among different final states.

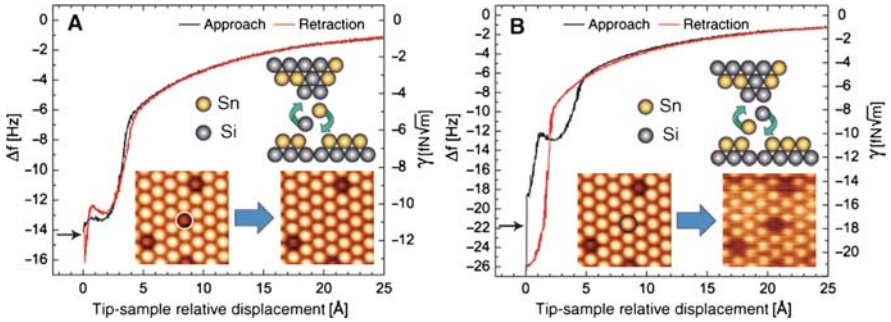

Fig. 11.8. (**a**) Characteristic frequency shift (Δf) signal on approach (*black*) and retraction (*red*) of the tip over an Si substitutional atom in an Sn/Si(111)-($\sqrt{3}\times\sqrt{3}$) surface during a vertical exchange manipulation. The *insets* display two consecutive topography images taken before and after the vertical manipulation, where the Si atom, marked with a *white circle*, was replaced by an Sn atom. (**b**) Characteristic frequency shift signal on approach (*black*) and retraction (*red*) of the tip above the Sn atom deposited in (**a**), pointed out by a *black circle*. In this case the Sn atom has been replaced by an Si atom coming from the tip

11.5.2 Dip-Pen Atomic Lithography: Vertical Atom Interchange Between the Tip and the Surface in the α-Sn/Si(111)-($\sqrt{3}\times\sqrt{3}$) Surface

The ability to incorporate individual atoms in a surface following predetermined arrangements might bring closer future atom-based technological enterprises. In this section, we discuss the basic atomistic mechanisms behind the recent experimental assembling of complex atomic patterns at RT by the vertical interchange of atoms between the tip-apex of an atomic force microscope and a semiconductor surface [16] (see Fig. 11.8). Our analysis will focus on the Sn/Si(111)-($\sqrt{3}\times\sqrt{3}$)R30° reconstruction, but these vertical interchange manipulations have also been reproduced in the Pb/Si(111)-($\sqrt{3}\times\sqrt{3}$)R30° and the In/Si(111)-($\sqrt{3}\times\sqrt{3}$)R30° reconstructions, where we expect the same mechanisms to be operative.

Although these experiments are discussed in detail in Chap. 8 of this volume, we provide here the basic experimental facts that are particularly relevant for the theoretical analysis. The inset of Fig. 11.8a shows topographic atomic resolution AFM images of a single atomic layer of tin atoms (bright protrusions) grown over a silicon (111) single crystal substrate. The dark spots correspond to substitutional silicon defects at the perfect tin surface layer. These Si defects can be vertically manipulated during force spectroscopy [13, 29] experiments. After imaging the surface and positioning the AFM tip with a lateral precision better than ± 0.1 Å [10] on top of the marked Si atom, the sample was progressively approached toward the oscillating AFM tip. At a given tip–surface distance, an instability in the frequency shift occurs as highlighted by the arrow in the graph. In the image taken immediately after

the sample retraction, the targeted Si atom has disappeared, and an Sn atom occupies the corresponding lattice position instead (right image in Fig. 11.8a). The only reasonable hypothesis to explain this event is that the Si atom at the surface has been replaced by an Sn atom originally located at the tip-apex, as sketched out by the cartoon in Fig. 11.8a. The same procedure can be consecutively applied to the freshly deposited Sn atom (marked with a circle in the left image of Fig. 11.8b), resulting in the replacement of this surface atom by an Si atom coming from the tip, and in a partial loss of atomic contrast (right image in Fig. 11.8b). The resemblance of the characteristic frequency shift curves (see Fig. 11.8) recorded on vertical atomic interchange manipulations performed on different experimental sessions with different tips is truly remarkable [16]. In spite of the apparent complexity of the process, this extremely good reproducibility strongly indicates the presence of a common basic microscopic mechanism.

The extensive force spectroscopy experiments on this surface show that 29% of the tips produced vertical interchange atom manipulation, being almost equally probable to find tips producing either Si deposition or alternate deposition of Sn and Si atoms (this is the case illustrated in Fig. 11.8), and less probable to have a tip depositing only Sn atoms. The preparation of these tips relies on making a number of gentle tip–surface contacts using the same cantilever over different measurement sessions, but there is no systematic way of producing a priori a particular kind of tip. Once an atom exchanging tip is found, it is possible to perform the manipulations in a reproducible way. Therefore, these vertical interchange atomic manipulations require a tip-apex rigid enough to endure the high loads over the repulsive part of the short-range chemical interaction without undergoing major structural modifications.

The creation of these atomic patterns must involve not only the repeated interchange of atoms between tip and surface but also diffusion and segregation processes at the tip-apex to guarantee the presence of the required chemical species in the appropriate atomic arrangement. The simulation of the whole process is far beyond the capabilities of current first-principles methods. Thus, we focus our analysis on the feasibility of the vertical atom interchange and the identification of the common atomistic mechanisms involved.

At this point, we still have to face the complexity of the phase-space that the closest tip and surface atoms can explore, with different possible outcomes including atom removal or deposition by the tip, apart from the vertical interchange. We have used the possibility to impose constraints on the tip model to further simplify the complex scenario associated with the tip mechanical response and separate the discussion in two different steps. First, we model the experimental apex with a rigid tip where only the two atoms defining the apex are allowed to relax on interaction with the surface (see Fig. 11.9). These simulations illustrate how the vertical interchange can take place at the atomic scale, and identify the crucial dimer structure formed by the closest tip and surface atoms. In a second step, we relax some of these constraints to show the interplay with the other possible final outcomes and processes and the role

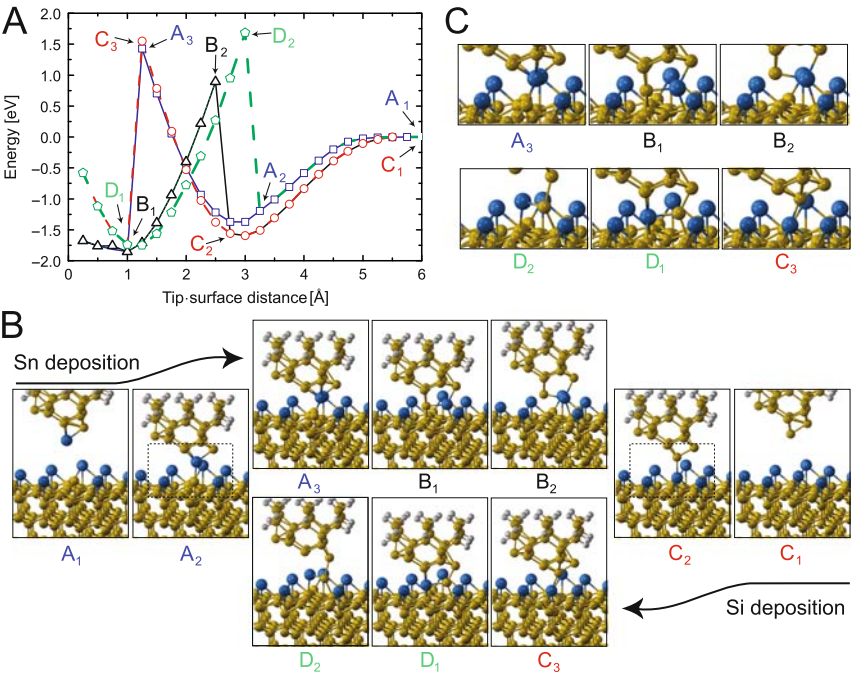

Fig. 11.9. First-principles simulations of the vertical interchange manipulation. (**a**) Evolution of the total energy on two consecutive tip approach and retraction cycles with a model rigid tip – only the two atoms in the dimer defining the apex are allowed to relax – over the same location of an Sn/Si(111)-($\sqrt{3} \times \sqrt{3}$)R30° surface resulting in the alternate deposition of an Sn atom (first cycle, *continuous lines*) and a Si atom (second cycle, *dashed lines*), respectively. (**b**) Atomic configurations associated with the transitions between energy branches labelled in (**a**) showing the relevant atomistic processes involved in the vertical interchange of atoms between tip and surface. (**c**) shows a zoom of the same selected configurations

of the temperature. In spite of its obvious limitations, our tip model captures an important property of the real tips, as a very robust apex is required to stand the high loads associated with the exploration of the repulsive part of the tip–surface short-range chemical interaction. This is the aspect that we have emphasized, sacrificing the quantitative description of the softer elastic response found in the experiments.

Figure 11.9 illustrates, using the total energy, the evolution of the system during an alternate deposition of an Sn (continuous lines) and an Si atom (dashed lines) using the rigid tip model. The most relevant atomic configurations during both processes are depicted in Fig. 11.9b. In the case of the Sn deposition, the system follows the branch A (squares), starting at A_1, where there is no significant interaction. At A_2, we are near the total energy minima and hence the zero of the short-range attractive force. Further tip–surface

approach leads to a repulsive force that increases up to structure A_3, where the atoms are significantly compressed but still keeping their original bonding topology. On retraction from any tip–surface distance larger than the one corresponding to A_3, the system follows the same energy curve back to the original structure A_1. On the contrary, approaching the tip beyond A_3, the system undergoes a discontinuous jump to a new energy branch B (triangles) with a significantly different bonding topology (panel B_1 in Fig. 11.9b). During further approach and consecutive retraction the system follows this energy branch up to B_2, where a new jump takes it to another energy solution (branch C, circles), leading to the final bonding topology (structure C_2) and the atomic interchange. The Si deposition case presents the same basic features. During approach, the system follows the C branch until reaching C_3, where it jumps to branch D (pentagons). Retraction from any distance along the D branch after this jump leads to a new jump from D_2 to A_2 and to the atom interchange. Comparing the two deposition cases, although the atomistic details are slightly different, overall, the atom interchange mechanism seems to be the same. The key step in these processes is to reach the earlier discussed *dimer-like* structure shown in panels B_1 and D_1. In these atomic configurations, the two original tip and surface closest atoms have now an "equal" number of bonds with the surrounding atoms, losing their identity as being part of the tip or the sample. Our simulations confirm that this dimer structure, that minimizes the stored elastic energy under compression, is the lowest energy configuration reached also with other tip–surface relative orientations and even with different tip structures.

Our DFT simulations using the rigid tip model reproduce the vertical interchange atom manipulations observed in the experiments and highlight the atomistic processes behind. The constraints imposed on the tip keep the energy barriers for all of the alternative processes – including tip modifications and extraction of atoms from the surface – quite high, while the barrier for the vertical interchange reduces significantly on loading. To further explore the role of the mechanical response of tip and the interplay among the different possible outcomes, we have approached our tip to a more realistic situation and carried out simulations with a setup, where the four outermost atoms of the tip-apex are allowed to relax. Figure 11.10a depicts the energy for an approach (squares) and retraction (triangles) cycle over an Si atom resulting in a tip change, where the Sn atom at the apex is lost and left on the surface. On retraction, the system crosses an energy branch (circles) that would result in the vertical interchange of these atoms – the Sn replaces the Si at the surface, while the Si atom incorporates into the dimer structure at the tip apex.

Given the complexity of the configuration space shown by these simulations, where an apparently small change in the tip leads to a completely different result for the approach/retraction curve, one may wonder about the feasibility of the vertical interchange. The important point to notice is also highlighted in Fig. 11.10a: all of the alternative outcomes lead the system to a final state of higher energy than the one associated with the vertical atom

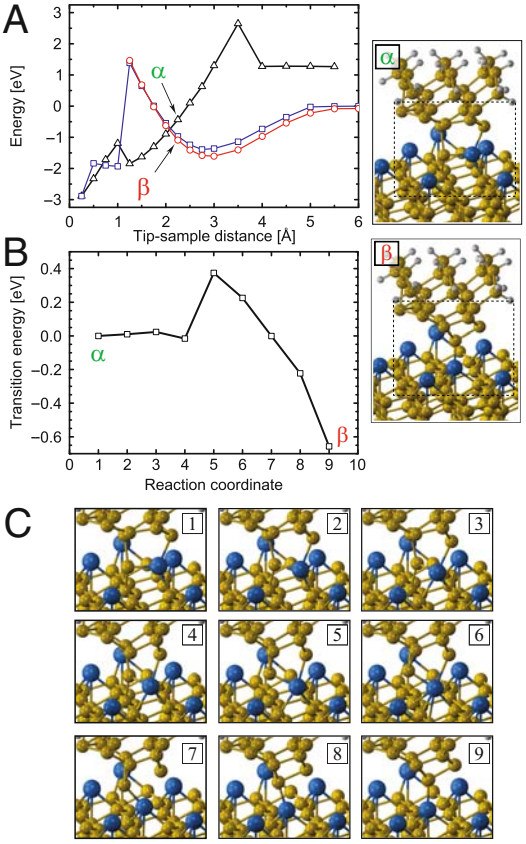

Fig. 11.10. (a) Total energy (*squares* and *triangles*) for a tip–surface approach and retraction cycle over an Si atom producing a tip modification where the Sn atom at the apex is lost and left on the surface. (**b**) Activation energy barrier between two atomic configurations close in total energy labelled as α and β in (**a**). The atomic configurations corresponding to the two α and β state are shown on the *right*. (**c**) Details of the bonding configurations along the minimum energy path for the transition from state α to state β

interchange. In the simulations discussed so far, where no temperature effects are included, the details of the tip structure and mechanical response determine which are the final states that can be reached without crossing significant energy barriers. However, in the experiments that are performed at room temperature, thermodynamics would favor the lowest energy final configurations. Therefore, the feasibility of the vertical interchange process is controlled by the energy barriers among the different local minima.

The calculation of the energy barriers in this multi-atom contact, where the structure of the transition state is difficult to guess, requires a more sophisticated approach that the constrained minimization used in the case of

the lateral manipulation. We have used the "Nudge Elastic Band" method [17], a well-established method for finding transition paths and the corresponding energy barriers between given initial and final states. In this method, a collection of intermediate sets of atomic configurations (or images) is created by a straight line interpolation of the coordinates of the atoms from the initial to the final state. Those images are connected together with springs to form a chain that provides a discrete representation of the path from the initial to the final state. This chain mimics an elastic band made of beads (the images) and springs. The total energy of the entire chain has to be minimized to find the minimum energy path (MEP). This total energy includes both the sum of the total energies of the different images and the contribution from the harmonic interaction between neighboring images along the direction of the path described by the chain. The minimization process involves the relaxation of the coordinates of the atoms in the different images subject to the constraints imposed by the springs. Any maximum along the MEP is a saddle point on the potential energy surface, and the energy of the highest saddle point gives the activation energy needed for the transition.

In our estimation of the typical barriers involved in vertical atom interchange processes, we have studied the transition of the system from an energy branch resulting in an Sn deposition to the one associated with the concerted vertical interchange. In particular, we have considered the transition energy between two atomic configurations very close in energy (points α and β in Fig. 11.10a) belonging to these two different branches: the starting atomic arrangement (α) is a dimer-like configuration in which both atoms have lost their identity as being part of the tip or the sample; the final state (β) is the deposition of the Sn atom. We have used nine images including the initial and final states labelled as α and β, respectively. Figure 11.10b displays the final energies for the sets of different atomic configurations defining the MEP. A zoom of the final relaxed structures over the relevant region of the tip–surface interface is displayed in Fig. 11.10c. We have found that there is an energy barrier of 0.4 eV for the transition between these two configurations (Fig. 11.10b), which is associated with the breaking of the remaining bond of the Si atom with the surface and the formation of a second bond of the Sn atom with the surface (see the panel labelled as 5 in Fig. 11.10c). With this relatively small energy barrier, these vertical interchange atom manipulations can easily take place at RT. It is not necessary to reach the high repulsive energies at which jumps between branches in Fig. 11.9 occur – energy values that would turn into extremely repulsive forces. In contrast, just driving the tip to tip–surface separations close (or slightly beyond) to the distance for the zero short-range force, we are very likely to obtain a vertical atomic interchange by a thermally activated jump near the crossing point of the different energy branches available for the system.

The simulations described earlier also shed light over some of the features exhibited by the associated experimental curves. The frequency shift signals (Fig. 11.8) display a shoulder at closer tip–surface distances, that develops into

a double well structure in the corresponding short-range chemical interaction forces (see Chap. 8). These features, together with the large energy dissipation measured at the closest tip–surface distances [24,28] can be qualitatively explained in terms of the presence of several energy branches – and, thus, different tip–surface interaction forces – during the evolution of the system. The energy barriers between branches as a function of the tip–surface distance dictate where the system jumps during either approach or retraction and, thus, determine the details of both frequency shift and force curves [16]. Since the frequency shift is proportional to a weighted average of the tip–surface interaction force over one oscillation cycle [30,31], the existence of these different force branches is blurred [24,28] in both the frequency shift and the short-range chemical interaction force derived from it; magnitudes that, a priori, only reflect the average conservative part of the interaction [30,32,33]. However, the calculated energy landscape provides a clear indication that the striking presence of two force minima of very similar depth are due to the evolution of the system between two different bonding configurations during an approach and retraction cycle.

Figure 11.11 shows the theoretical results that explain the origin of the dissipation signal and the force spectroscopy results measured in the experiments. An oscillation cycle of the experimental approach curve shown in Fig. 11.8b, before reaching the point of maximum proximity between tip and surface, can be simulated by assuming that: (1) the tip approaches the surface following energy branch C in Fig. 11.9; (2) at a given tip–surface distance (C_3), the system jumps to the energy branch D; and (3) on retraction the

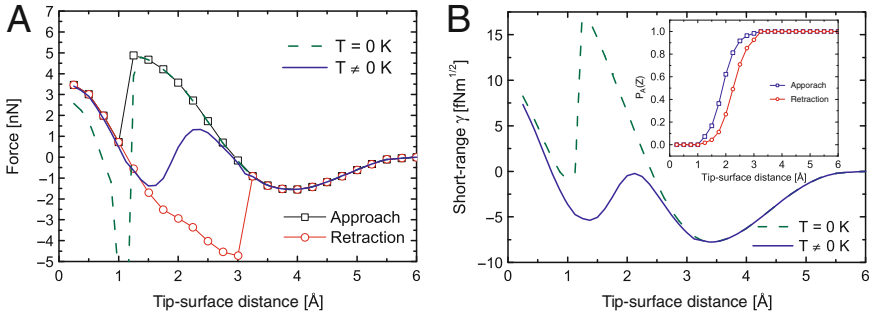

Fig. 11.11. (**a**) Short-range forces corresponding to the evolution and transitions between the energy branches C and D shown in Fig. 11.9; *squares* and *circles* denote the force upon approach and retraction, respectively. The theoretical forces that would be obtained from the inversion of the frequency shift at zero (*dashed*) and non-zero (*continuous*) temperature are also included. (**b**) Normalized frequency shift obtained from the short range force curves shown in (**a**) at zero (*dashed line*) and nonzero temperature (*continuous line*). The *inset* displays the probability of being in the C branch during the approach–retraction cycle used to incorporate the effect of a nonzero temperature in the frequency shift calculation

system jumps back (D_2) to the branch C. Notice that, in this case, there is not vertical atomic interchange and therefore the initial and final configuration upon approach and retraction are identical. The forces on approach (squares) and retraction (circles), assuming these transitions between energy branches, are shown in Fig. 11.11a. An approach and retraction cycle considering these two force solutions leads to a dissipated energy of $\sim$7 eV. The normalized frequency shift γ associated with this process is shown in Fig. 11.11b (dashed line). The step-like change of γ at the tip–surface distance where the atom reallocations take place is an expected consequence of the force hysteresis. The green dashed line of Fig. 11.11a is the force curve associated to this normalized frequency shift when it is calculated with the same inversion procedure used with the experimental results. This curve coincides with the force of the C branch before the jump (up to this point, the force over the oscillation cycle is conservative), but, for closer distances, a strong hysteresis (jump) appears and the short-range force calculated from the frequency shift inversion loses its meaning [30, 32, 33].

Both the force curve and the dissipated energy ($\sim$7 eV) associated with this process are still quite different from the experimental ones. The origin of this discrepancy lays on the role played by the temperature: our calculations so far are done at zero temperature while the experiments are performed at RT. At finite temperature, the system can overcome energy barriers between different energy solutions that smears out the steps and reduces the dissipation signal found at zero temperature [28]. To incorporate the effect of the temperature, we have calculated the normalized frequency shift (continuous line in Fig. 11.11b) using the force solutions on approach and retraction shown in Fig. 11.11a, but giving them some relative probabilities (see the inset of Fig. 11.11b) that reproduce the measured dissipation energy ($\sim$1.2 eV) at the closer tip–surface distances. The corresponding short-range force curve (continuous line in Fig. 11.11a) obtained from this frequency shift using the inversion procedure [31] now exhibits the main feature of the experimental forces: a double well with similar force minimum values. Therefore, this characteristic feature in the experimental short-range force curve is a clear signature of force hysteresis during the approach and retraction cycle.

11.6 Conclusion

This chapter unveils the atomic-scale mechanisms that are responsible for the RT manipulations of strongly bound atoms on semiconductor surfaces. First-principles simulations, matching the experimental forces, identify the key steps in two paradigmatic examples: the lateral manipulation of single adatom vacancies on the Si(111)-7×7 reconstruction in the attractive regime, and the vertical interchange of atoms between the tip and the Sn/Si(111)-$(\sqrt{3} \times \sqrt{3})$R30° surface by a gentle exploration of the repulsive force regime. Our calculations reveal that the outstanding experimental control of the

manipulation under attractive forces comes from the localized reduction of the diffusion energy barriers induced by the tip for the different steps in the complex path followed by the Si adatom during the process. Using selective constraints to face the difficulties posed by the complexity of a multi-atom contact and operation in the repulsive regime, our simulations illustrate how the vertical interchange can take place at the atomic scale, identify the crucial dimer structure formed by the closest tip and surface atoms, and discuss the role of temperature in the competition with other possible final outcomes (including atom removal or deposition by the tip).

Acknowledgements

The authors acknowledges the relevant experimental contribution from Oscar Custance, Yoshiaki Sugimoto, Masayuki Abe and Prof. Seizo Morita to the work described in this chapter. The work of P.P. and R.P. is supported by the Ministerio de Ciencia e Innovacion (MICINN, Spain) under Grants MAT2005-01298 and NAN2004-09183-C10, and by the VI Framework Programme of the European Union under the STREP project FORCETOOL (NMP4-CT-2004-013684). P.P. acknowledges the financial support by the Juan de la Cierva Programme (MICINN, Spain). P.J. acknowledges the financial support from COST P19-OC09028 and GAAV under the grants no. IAA 100100905 and GA CR 202/09/0775. Part of these calculations has been performed at the Centro de Computacion Cientifica of the UAM and the MareNostrum supercomputer at the BSC-CNS.

References

1. D. Eigler, E.K. Schweizer, Nature **344**, 524 (1990)
2. F. Giessibl, Science **267**, 68 (1995)
3. N. Oyabu, O. Custance, I. Yi, Y. Sugawara, S. Morita, Phys. Rev. Lett. **90**(17), 176102 (2003)
4. S. Morita, I. Yi, Y. Sugimoto, N. Oyabu, R. Nishi, O. Custance, M. Abe, Appl. Surf. Sci. **241**, 2 (2005)
5. S. Kawai, H. Kawakatsu, Appl. Phys. Lett. **89**, 023113 (2006)
6. N. Oyabu, Y. Sugimoto, M. Abe, O. Custance, S. Morita, Nanotechnology **16**(3), S112 (2005)
7. Y. Sugimoto, M. Abe, S. Hirayama, N. Oyabu, O. Custance, S. Morita, Nat. Mater. **4**(2), 156 (2005)
8. R. Nishi, D. Miyagawa, Y. Seino, I. Yi, S. Morita, Nanotechnology **17**(7), S142 (2006)
9. S. Hirth, F. Ostendorf, M. Reichling, Nanotechnology **17**(7), S148 (2006)
10. M. Abe, Y. Sugimoto, O. Custance, S. Morita, Appl. Phys. Lett. **87**(17), 173503 (2005)
11. M. Abe, Y. Sugimoto, O. Custance, S. Morita, Nanotechnology **16**(12), 3029 (2005)

12. M. Abe, Y. Sugimoto, T. Namikawa, K. Morita, N. Oyabu, S. Morita, Appl. Phys. Lett. **90**(20), 203103 (2007)
13. Y. Sugimoto, P. Pou, M. Abe, P. Jelinek, R. Pérez, S. Morita, O. Custance, Nature **446**, 64 (2007)
14. M. Ternes, C. Lutz, C. Hirjibehedin, F. Giessibl, A. Heinrich, Science **319**, 1066 (2008)
15. Y. Sugimoto, P. Jelinek, P. Pou, M. Abe, S. Morita, R. Pérez, O. Custance, Phys. Rev. Lett. **98**, 106104 (2007)
16. Y. Sugimoto, P. Pou, O. Custance, P. Jelínek, M. Abe, R. Pérez, S. Morita, Science **322**, 413 (2008)
17. G. Henkelman, H. Jónsson, J. Chem. Phys. **113**, 9901 (2000)
18. R. Martoňák, D. Donadio, A. Oganov, M. Parrinello, Nat. Mater. **5**, 623 (2006)
19. P. Dieska, I. Štich, R. Pérez, Phys. Rev. Lett. **95**(12), 126103 (2005)
20. P. Dieska, I. Stich, Nanotechnology **18**, 084016 (2007)
21. O.F. Sankey, D.J. Niklewski, Phys. Rev. B **40**(6), 3979 (1989)
22. P. Jelinek, H. Wang, J.P. Lewis, O.F. Sankey, J. Ortega, Phys. Rev. B **71**(23), 235101 (2005)
23. M. Basanta, Y.J. Dappe, P. Jelinek, J. Ortega, Comp. Mat. Sci. **39**, 759 (2007)
24. N. Oyabu, P. Pou, Y. Sugimoto, P. Jelinek, M. Abe, S. Morita, R. Pérez, O. Custance, Phys. Rev. Lett. **96**(10), 106101 (2006)
25. Y. Sugimoto, O. Custance, S. Morita, M. Abe, P. Pou, P. Jelínek, R. Pérez, Phys. Rev. B **73**, 205329 (2006)
26. R. Pérez, M. Payne, I. Štich, K. Terakura, Phys. Rev. Lett. **78**(4), 678 (1997)
27. P. Jelínek, M. Švec, P. Pou, R. Perez, V. Cháb, Phys. Rev. Lett. **101**, 176101 (2008)
28. L.N. Kantorovich, T. Trevethan, Phys. Rev. Lett. **93**(23), 236102 (2004)
29. M.A. Lantz, H.J. Hug, R. Hoffmann, P.J.A. van Schendel, P. Kappenberger, S. Martin, A. Baratoff, H.J. Güntherodt, Science **291**(5513), 2580 (2001)
30. F.J. Giessibl, Phys. Rev. B **56**(24), 16010 (1997)
31. J.E. Sader, S.P. Jarvis, Appl. Phys. Lett. **84**(10), 1801 (2004)
32. H. Hölscher, B. Gotsmann, W. Allers, U.D. Schwarz, H. Fuchs, R. Wiesendanger, Phys. Rev. B **64**(7), 075402 (2001)
33. U. Dürig, Appl. Phys. Lett. **75**(3), 433 (1999)